SANDIA REPORT
SAND2017-11781
Unlimited Release
Printed October 2017XX

Tunneling-assisted transport of carriers through heterojunctions

Samuel M. Myers, Normand A. Modine and William R. Wampler

Prepared by
Sandia National Laboratories
Albuquerque, New Mexico 87185 and Livermore, California 94550

Sandia National Laboratories is a multi-mission laboratory managed and operated by National Technology and Engineering Solutions of Sandia, LLC, a wholly owned subsidiary of Honeywell International, Inc., for the U.S. Department of Energy's National Nuclear Security Administration under contract DE-NA0003525.

Issued by Sandia National Laboratories, operated for the United States Department of Energy by National Technology and Engineering Solutions of Sandia, LLC.

Available to DOE and DOE contractors from
U.S. Department of Energy
Office of Scientific and Technical Information
P.O. Box 62
Oak Ridge, TN 37831

Telephone: (865) 576-8401
Facsimile: (865) 576-5728
E-Mail: reports@osti.gov
Online ordering: http://www.osti.gov/scitech

Available to the public from
U.S. Department of Commerce
National Technical Information Service
5301 Shawnee Rd
Alexandria, VA 22312

Telephone: (800) 553-6847
Facsimile: (703) 605-6900
E-Mail: orders@ntis.gov
Online order: http://www.ntis.gov/search

SAND2017-11781
Printed October 2017XX
Unlimited Release

Tunneling-assisted transport of carriers through heterojunctions

Samuel M. Myers
Radiation-Solid Interactions Department 1884

Normand A. Modine
Nanostructure Physics Department 1864

William R. Wampler
Radiation-Solid Interactions Department 1884

Sandia National Laboratories
P. O. Box 5800
Albuquerque, New Mexico 87185-MS1056

Abstract

The formulation of carrier transport through heterojunctions by tunneling and thermionic emission is derived from first principles. The treatment of tunneling is discussed at three levels of approximation: numerical solution of the one-band envelope equation for an arbitrarily specified potential profile; the WKB approximation for an arbitrary potential; and, an analytic formulation assuming constant internal field. The effects of spatially varying carrier chemical potentials over tunneling distances are included. Illustrative computational results are presented. The described approach is used in exploratory physics models of irradiated heterojunction bipolar transistors within Sandia's QASPR program.

TABLE OF CONTENTS

1. INTRODUCTION

Currents in heterojunction bipolar transistors (HBTs) are affected by band offsets at the heterojunction. Consequences can be particularly significant for majority carriers emerging from the emitter into the base, because such carriers encounter a potential-energy peak arising from the combined influences of the band offset and the internal field. This is depicted schematically in Fig. 1 for the case of conduction electrons near a forward-biased n-p heterojunction, where the potential energy corresponds to the conduction-band edge. In modeling Sandia HBTs [1,2], we have largely adopted a common description of the cross-junction transport [3,4] based on thermionic-emission and tunneling in the WKB approximation with the assumption of Boltzmann carrier statistics. We elaborated this treatment by forgoing the assumption of constant carrier chemical potential along the ramp of the potential peak [2]. Our resulting simulations of HBTs, using literature values for material parameters, generally yield collector currents in approximate agreement with experiment, so that device modeling can be accomplished with minor calibration adjustments.

The purposes of the present report are, first, to derive and document the above aspects of our device modeling; and, second, to assess the accuracy of simplifying approximations related to tunneling. As part of the latter task, we compute carrier wave functions by numerically solving the one-band envelope equation, yielding a tunneling transmission coefficient more accurate than that from the WKB approximation. The numerical determinations of the wave functions and the energy-dependent transmission coefficient are described in Sect. 2. Comparisons are made with the WKB approximation. In Sect. 3, the carrier flux is formulated in terms of the transmission coefficient obtained in Sect. 2. Illustrative computational results are presented. Conclusions and implications are discussed in Sect. 4.

2. WAVE FUNCTIONS AND THE TUNNELING TRANSMISSION COEFFICIENT

Planer device symmetry is assumed, allowing the use of one-dimensional wave functions for this part of the development. The one-band envelope equation for carriers, with the effective-mass approximation, has the form of the Schrödinger equation:

$$-\frac{\hbar^2}{2m}\frac{d^2}{dx^2}\Psi(x)=\left[E-U(x)\right]\Psi(x) \quad . \tag{1}$$

Here Ψ is the longitudinal, x-axis part of the 3-D wave function, E is the corresponding component of state energy, m is the effective carrier mass, and $\hbar$ is Planck's constant divided by 2π; U is the potential energy, corresponding to the band edge for conduction electrons and its negative for holes, which varies with location along the x axis. The effect of the modest change in effective mass at the junction is neglected.

For purposes of numerical solution, the region of varying potential U(x) containing the heterojunction is artificially bracketed by intervals of constant potential, U_L on the left and U_R on the right. Thus, an actual potential profile resembling that of Fig. 1 is modified as shown in Fig. 2. In the region of constant potential on the left, the solution has the general form

$$\Psi(x)=Ae^{iK_Lx+i\alpha}+Be^{-iK_Lx+i\beta} \tag{2}$$

where A and B are real, phase offsets are represented by the terms $i\alpha$ and $i\beta$ in the exponents, and K_L is given by

$$K_L=\frac{\sqrt{2m\left(E-U_L\right)}}{\hbar} \quad . \tag{3}$$

The first exponential term in Eq. (2) describes a particle wave incident from the left, while the second term represents the reflected component. Within the plateau on the right, we consider the case where only the transmitted component of the impinging wave is present:

$$\Psi(x)=Ce^{iK_Rx+i\gamma} \tag{4}$$

with C real and

$$K_R=\frac{\sqrt{2m\left(E-U_R\right)}}{\hbar} \quad . \tag{5}$$

The particle flux associated with an individual wave function is given in general by [5]

$$\Phi=\frac{\hbar}{2mi}\left(\Psi^*\frac{d\Psi}{dx}-\frac{d\Psi^*}{dx}\Psi\right) \tag{6}$$

which for the simple wave function in Eq. (4) reduces to

$$\Phi = C^2 \frac{\hbar}{m} K_R \quad . \tag{7}$$

The invariance of $\Phi(x)$ versus x required by particle conservation provides a check on numerical solutions for the wave function.

The energy-dependent transmission coefficient characterizing band-to-band tunneling through the barrier is defined as the ratio of the transmitted flux to the incident flux, and is given by

$$T_{bb}(E) = \frac{C^2 K_R}{A^2 K_L} \quad . \tag{8}$$

The procedure to determine this quantity has three parts: 1) choose an amplitude C and a phase γ at a location x_1 within the potential plateau to the right of the barrier; 2) numerically integrate Eq. (1) from x_1 through the barrier into the region of constant potential on the left; and 3) extract the coefficient A from the resultant $\Psi(x)$ on the left. This calculation is performed for energies E greater than both U_L and U_R.

The numerical integration is performed from right to left in order to initialize within the region where the solution has a single component. To this end the x axis is discretized with a constant (negative) step $-\Delta x$. Approximating the derivative of Eq. (1) in terms of finite differences gives

$$\Psi_i = \left[2 - \frac{2m}{\hbar^2} \left(E - U_{i-1} \right) \left(\Delta x \right)^2 \right] \Psi_{i-1} - \Psi_{i-2} \quad \text{for } i \geq 3 \quad . \tag{9}$$

In order to compute using real numbers, we separate the discretized wave function into real and imaginary components as

$$\Psi_i = \varphi_i^r + i\varphi_i^i \tag{10}$$

where $\varphi^r(x)$ and $\varphi^i(x)$ are real and are independent solutions of Eqs. (1). The full solution is then obtained by separate integrations for the two components.

Initiating the integration on the right side of the peak avoids complexities arising from the presence of two wave-function components in Eq. (2). A convenient starting specification is $\Psi_1 = 1$, corresponding to C = 1 and $\gamma = -K_R x_1$. Making use of Eqs. (4) and (10), one then obtains

$$\begin{aligned} \varphi_1^r &= 1 \quad \varphi_1^i = 0 \\ \varphi_2^r &= \cos(K_R \Delta x) \quad \varphi_2^i = -\sin(K_R \Delta x) \end{aligned} \quad . \tag{11}$$

The range of integration is chosen to encompass more than one oscillation cycle on the left side of the peak for all K_L of interest.

To determine T_{bb} from the numerically obtained wave function $\Psi(x)$, it is necessary to separate the contributions of the two terms in Eq. (2) and thereby evaluate the coefficient A. This is accomplished by extracting two quantities from the numerical results on the left side of the peak that, on the basis of Eq. (2), depend differently on A and B. These quantities are the average squared magnitude of Ψ and the net particle flux Φ. Using Eqs. (2) and (10), it can be shown that

$$\frac{K_L}{\pi}\int_{x_0}^{x_0+\pi/K_L}\left[\Psi^*\Psi\right]dx = \frac{K_L}{\pi}\int_{x_0}^{x_0+\pi/K_L}\left[\left(\varphi^r\right)^2+\left(\varphi^i\right)^2\right]dx = A^2 + B^2 \tag{12}$$

in the left plateau region. From Eqs. (2), (6) and (10) one has

$$\Phi = \frac{\hbar}{2mi}\left(\Psi^*\frac{d\Psi}{dx} - \frac{d\Psi^*}{dx}\Psi\right) = \frac{\hbar}{m}\left(\varphi_r\frac{d\varphi_i}{dx} - \frac{d\varphi_r}{dx}\varphi_i\right) = \frac{\hbar}{m}K_L\left(A^2 - B^2\right) \tag{13}$$

in the same region, where the derivatives are given in terms of finite differences as

$$\frac{d}{dx}\varphi(x_i) = \frac{\varphi_{i+1} - \varphi_{i-1}}{2\Delta x} \quad . \tag{14}$$

Combining Eqs. (12) and (13) gives A^2 in terms of the numerically determined φ_i^r and φ_i^i, yielding $T_{bb}(E)$ via Eq. (8).

A verification test of the above numerical procedure is provided by comparing to analytic results for a rectangular barrier with $U_L = U_R$ and impinging carrier kinetic energies, E - U_L,

that are less than the barrier height. Joining relations between wave functions in the three x-axis intervals of this configuration have been derived elsewhere [6], yielding equations that determine the transmission coefficient. Such a comparison is shown in Fig. 3 for a barrier of height 0.2 eV and width 10 nm with a normalized carrier effective mass of 0.1. The numerical calculation was performed with $\Delta x = 0.01$ nm. The numerical and analytic results are accurately consistent.

The potential profile U(x) near heterojunctions in bipolar devices resembles the idealized, triangular shape of Figs. 1 and 2, but the ramp depicted as a straight line actually has a varying slope due to the decrease of the internal field with distance from the junction. In this situation, three levels of accuracy can be considered for the calculation of the tunneling transmission coefficient pursuant to the evaluation of device current. The most accurate method is the approach discussed above based on the numerical solution of Eq. (1). A simpler alternative, although still requiring numerical integration, is to employ the WKB approximation [7]:

$$T_{bb}(E) = \exp\left\{-\frac{2\sqrt{2m}}{\hbar}\int_{x_E}^{x_{max}}\sqrt{U(x)-E}\;dx\right\} \tag{15}$$

where the subscript max indicates the values of quantities at the apex of the peak, and x_E is the value of x along the ramp where U(x) = E. A widely used further simplification is to assume that the internal field F is constant over relevant tunneling distances, so that U(x) varies linearly with x. Equation (15) then reduces to

$$T_{bb}(E) = \exp\left\{-\frac{4\sqrt{2m}}{3\hbar qF}\left[U_{max}-E\right]^{3/2}\right\} \tag{16}$$

where q is the elementary charge. In modeling Sandia HBTs [1,2], we have employed Eq. (15) to accommodate instances where the spatial variation of the internal field is consequential.

In order to assess the adequacy of Eq. (15) for present purposes, we compare with results from the numerical, wave-function approach. Since the principal issue is the accuracy of the WKB approximation, it suffices to perform these calculations for the situation of constant field.

We treat a triangular barrier with F = 10 MV/m and $U_{max} = 0.2$ eV and a normalized effective mass of 0.1. The specified field is representative of devices, while the peak amplitude is somewhat larger for purposes of illustration. Results for the energy-dependent transmission

coefficient are shown in Fig. 4 using linear and logarithmic vertical scales. Differences range up to about a factor of two.

3. DEVICE CURRENTS

Whereas the transmission coefficient for a single carrier state was evaluated in one dimension, the combined flux of carriers traversing the barrier involves an ensemble of 3-D band states, whose occupation probabilities depend on total state energy and the chemical potential of the carriers. We consider this problem for a structure having planer symmetry: the potential plateau to the left of the barrier in Fig. 2 extends for a distance L_{wf} much greater than the width of the barrier, while the lateral, y and z ranges, with invariant U(x), also span distances of L_{wf}. Within the plateau region of volume $V_{wf} = L_{wf} \times L_{wf} \times L_{wf}$ where $U(x) = U_L$, the normalized wave functions are accurately approximated as [8]

$$\Psi(x,y,z) = \Psi_x(x)\Psi_y(y)\Psi_z(z) = \frac{e^{iK_x x}}{L_{wf}^{1/2}} \frac{e^{iK_y y}}{L_{wf}^{1/2}} \frac{e^{iK_z z}}{L_{wf}^{1/2}} \tag{17}$$

for periodic boundary conditions, neglecting the relatively small contribution to the volume integral from the barrier region. The allowed K values for the three axes range from $-\infty$ to $+\infty$, and are separated by a constant interval of $2\pi/L_{wf}$. Spin degeneracy increases the number of 3-D states by a factor of 2. The associated axial energies are given by

$$\begin{aligned} E_x &= \frac{\hbar^2 K_x^{\,2}}{2m} + U_L \\ E_{y,z} &= \frac{\hbar^2 K_{y,z}^{\,2}}{2m} \end{aligned} \tag{18}$$

with total energy E equal to the sum of the three. Transmission from left to right through the barrier region occurs only for positive K_x such that E_x is greater than both U_L and U_R. Defining a minimum energy E_{x0} as the larger of U_L and U_R, this implies that $K_x > K_{x0}$ where

$$K_{x0} = \frac{\sqrt{2m\left(E_{x0} - U_L\right)}}{\hbar} \quad . \tag{19}$$

From Eq. (6), the particle flux along the x axis for an individual state is

$$\Phi_x = \frac{\hbar K_x}{m V_{wf}} \quad . \tag{20}$$

The density of such states in $\{K_X,K_Y,K_Z\}$ space is $V_{wf}/(8\pi^3)$.

We employ the large-volume eigenstates of Eq. (17) while recognizing that scattering events limit wave-function coherence to microscopic distances. This choice removes the need to solve Eq. (1) iteratively as an eigenvalue problem, allowing instead the use of known energy eigenvalues for the bulk, which greatly expedites the calculations. In earlier studies concerned with the tunneling of carriers to defect traps [1,2,9], we compared predicted rates obtained with such bulk eigenstates to results from local-state calculations, and found good agreement. Key to this consistency are compensating scaling effects of the number of eigenstates and their wavefunction amplitudes.

Energy-dependent occupation probabilities for the carrier states are computed here assuming Boltzmann rather than Fermi-Dirac statistics. This is justified in modeling HBTs because relevant concentrations near the heterojunction are small compared to the band effective density of states, in marked contrast to the situation for trapping at defects [1,2]. The occupation probability is then given by

$$P(E) = \exp\left(\frac{\phi - E}{k_B T}\right) \tag{21}$$

where ϕ is the chemical potential, k_B the Boltzmann constant, and T the temperature. As a first approximation it can be assumed that ϕ is invariant, although this quantity necessarily varies with x in a biased device with current flowing. Our simulations typically show differences of several times k_BT between contacts [2]. We have elected to include a first-order correction for this effect as follows: for $U_L < E < U_{max}$, the employed value of $\phi(x)$ is that at the intersection of E and U(x); whereas, for $E \geq U_{max}$, the value at the peak is used. This dependence will be represented by the function $\phi_E(E)$.

Combining the above elements and integrating over $\{K_X,K_Y,K_Z\}$ space yields the total flux of carriers from left to right through the barrier region:

$$J_{bb}[L \Rightarrow R] =$$

$$2\int_{-\infty}^{+\infty}\int_{-\infty}^{+\infty}\int_{K_{x0}}^{+\infty}\frac{\hbar K_x}{m V_{wf}}T_{bb}(E_x)\exp\left(\frac{\phi_E(E_x)-E_x-E_y-E_z}{k_B T}\right)\frac{V_{wf}}{8\pi^3}dK_x dK_y dK_z \quad . \tag{22}$$

The factor of 2 takes account of spin degeneracy. The three axial integrals are separable, a large computational benefit from the use of Boltzmann statistics. Evaluating the transverse integrals and changing variables from K_X to E_X, we obtain

$$J_{bb}[L \Rightarrow R] = \frac{m k_B T}{2\pi^2\hbar^3}\int_{E_{x0}}^{+\infty}T_{bb}(E_x)\exp\left(\frac{\phi_E(E_x)-E_x}{k_B T}\right)dE_x \quad . \tag{23}$$

When the WKB approximation is used to compute the transmission coefficient, so that $T_{bb} = 1$ for $E > U_{max}$, there is a straightforward separation between the regimes of tunneling and thermionic emission without tunneling. When in addition $\phi_E(E_X)$ is replaced by a constant chemical potential ϕ, Eq. (23) becomes consistent with earlier treatments of thermionic emission and tunneling through junctions with barriers [3,4].

Figure 5 shows incremental fluxes $\Delta J_{bb}[L=>R]$ from the integration of Eq. (23) for a triangular potential like that in Fig. 2 with normalized effective mass = 0.1, T = 300 K, field = 10 MV/m, $U_L = U_R$, and $U_{max} - U_L = 0.2$ eV. The displayed results utilize the two transmission coefficients plotted in Fig. 4, which were respectively computed using the wave-function approach and the WKB approximation. The curves differ significantly at particular energies, but their areas, and hence the carrier fluxes, agree to about 2%. This is evidence for the adequacy of the WKB method for many purposes.

The reverse carrier flux, going from right to left, is included in device modeling. We formulate this contribution for the triangular potential configuration of Fig. 2 by assuming that the prefactor and transmission coefficient in Eq. (23) have the same values, and further that the net incremental flux at each value of E_X goes to zero when $\phi_E(E_X) = \phi_R$, where the latter chemical potential is adjacent to the junction on the right side. These stipulations are satisfied by the following equation for the net combined flux:

$$J_{bb} = \frac{m k_B T}{2\pi^2 \hbar^3} \int_{E_{x0}}^{+\infty} T_{bb}(E_x) \left[\exp\left(\frac{\phi_E(E_x) - E_x}{k_B T} \right) - \exp\left(\frac{\phi_R - E_x}{k_B T} \right) \right] dE_x \quad . \tag{24}$$

In simulations of HBTs we generally employ the effective mass from the left side of the heterojunction, both in Eq. (24) and in the calculation of the transmission coefficient, because the potential peak is on that side. A detailed treatment of the effective-mass offset, while feasible, was not deemed worthwhile. The evaluations of the local chemical potentials $\phi_E(E_x)$ and ϕ_R from local carrier concentrations use the local masses on the respective sides. In the case of light and heavy holes, whose effective masses differ by a large multiple, tunneling − but not thermionic emission − is assumed to occur entirely via the light species.

4. CONCLUSION

The formulation of band-to-same-band tunneling used to model Sandia HBTs was reinforced by derivation from first principles. Calculation of the transmission coefficient via the WKB approximation was assessed by comparison to numerical solutions of the one-band envelope equation, and was deemed acceptable for device-relevant conditions. Our earlier, plausible extension of device models to accommodate tunneling from spatially varying carrier chemical potentials was shown to be rigorous.

.

ACKNOWLEDGMENTS

This work was conducted as part of the exploratory physics development supporting computational simulations for the QASPR (Qualification Alternatives to the Sandia Pulsed Reactor) project, and was supported by the Sandia Advanced Simulation and Computing Physics and Engineering Models program.

REFERENCES

1. S. M. Myers, W. R. Wampler, and N. A. Modine, *Recombination by band-to-defect tunneling near heterojunctions in irradiated bipolar devices: a theoretical model*, Sandia Report SAND2015-7650.
2. S. M. Myers, W. R. Wampler, and N. A. Modine, J. Appl. Phys. **120**, 134502 (2016).
3. D. Schroeder, Modeling of Interface Carrier Transport for Device Simulation (Springer, 1994), pp. 154 - 171.
4. S. M. Sze and K. K. Ng, Physics of Semiconductor Devices (Wiley, 2007), pp. 154 - 164.
5. E. Merzbacher, Quantum Mechanics (Wiley, 1964), pp. 37 - 38.
6. Ibid., pp. 91 - 93.
7. S. M. Sze and K. K. Ng, Physics of Semiconductor Devices (Wiley, 2007), pp. 47 - 48.
8. E. Merzbacher, Quantum Mechanics (Wiley, 1964), pp. 200 - 203.
9. S.M. Myers, W.R. Wampler and N.A. Modine, *Probability density of tunneled carrier states near heterojunctions calculated numerically by the scattering method,* Sandia Report SAND2017-10494

FIGURES

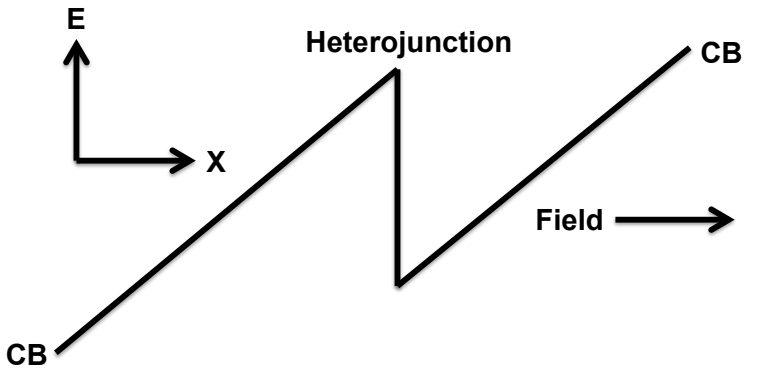

Fig. 1. Conduction-band edge near an n-p heterojunction.

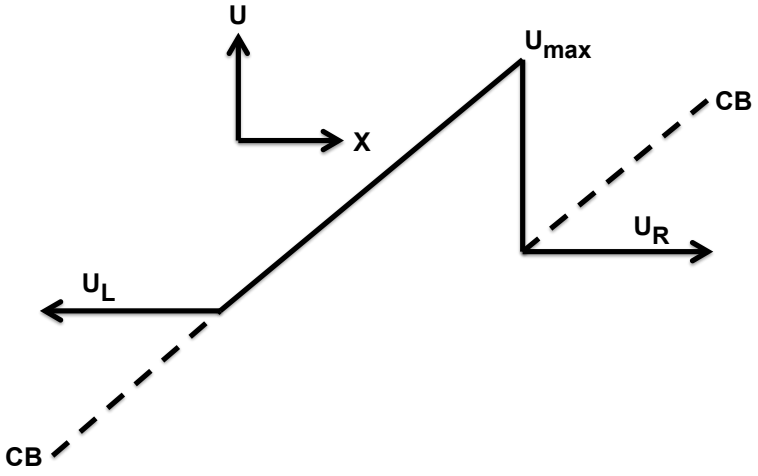

Fig. 2. Potential profile used in the numerical solution of Eq. 1. The region of varying U(x) is artificially extended by plateaus to produce bounding regions where the wave function has simple form.

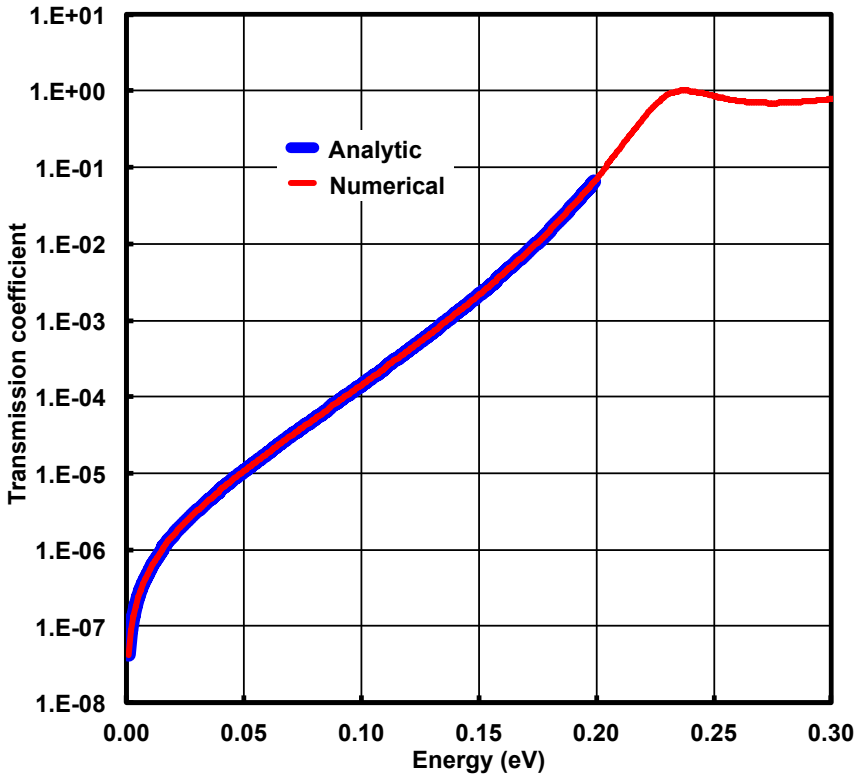

Fig. 3. Transmission coefficient for a rectangular barrier, as calculated analytically and using the numerical procedure of Sect. 2. The height of the barrier is 0.2 eV, the width is 10 nm, and the normalized carrier mass is 0.1.

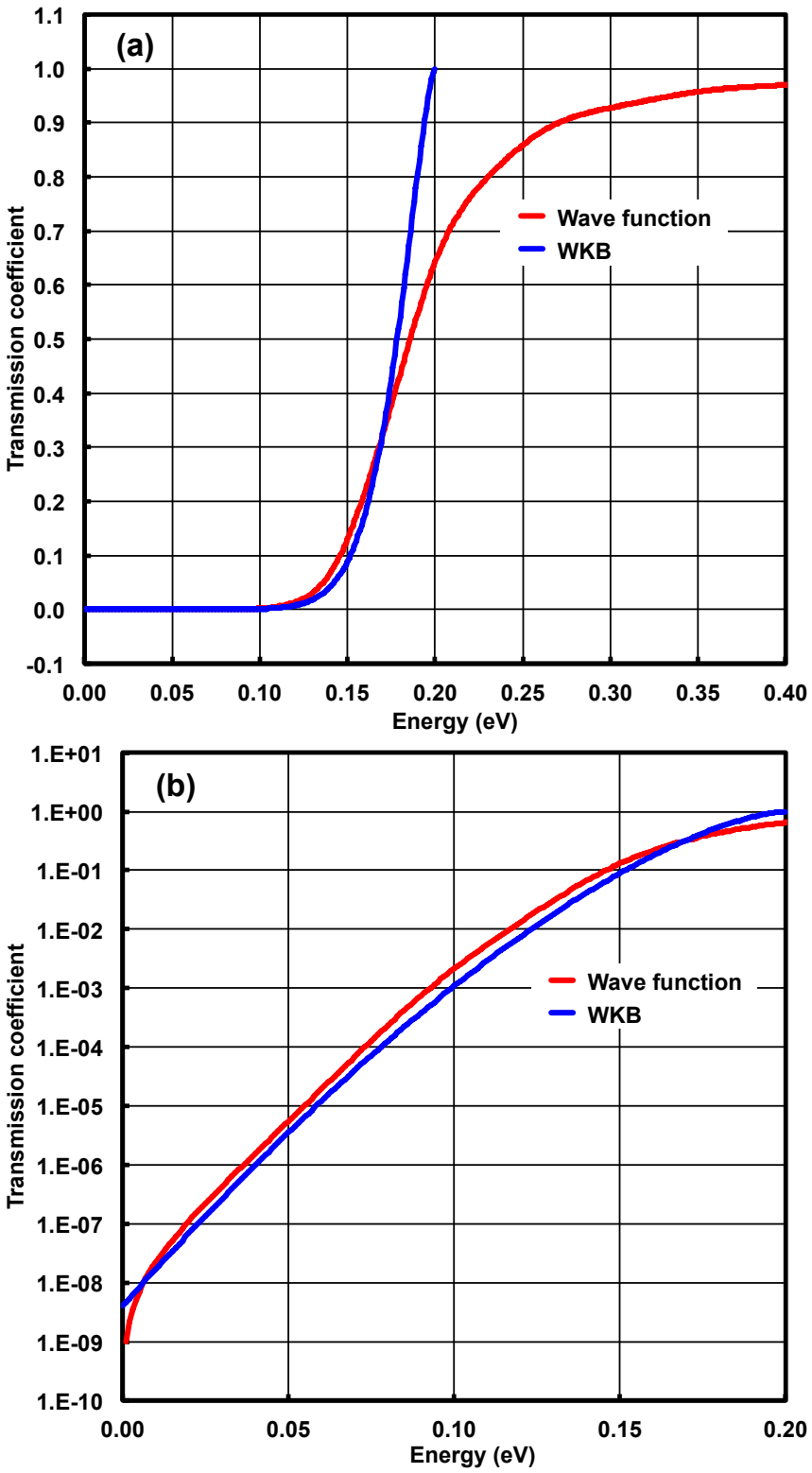

Fig. 4. Transmission coefficient for a triangular barrier as calculated using the numerical, wave-function procedure of Sect. 2 and the WKB approximation. The height of the barrier is 0.2 eV, the width is 20 nm, and the normalized carrier mass is 0.1. Results are displayed in linear (a) and semi-log (b) formats.

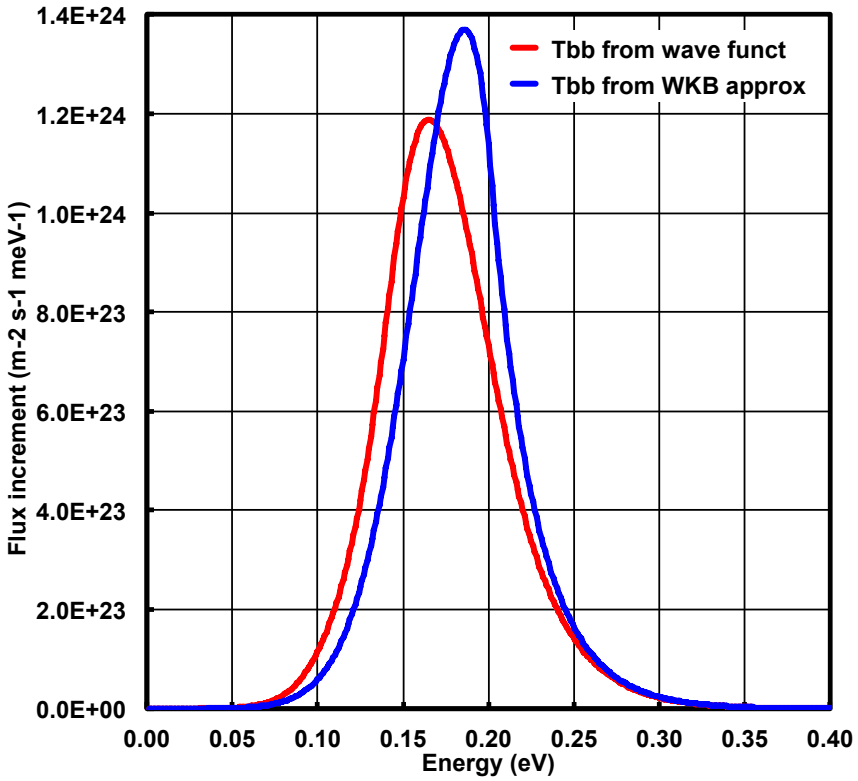

Fig. 5. Tunneled-flux increments from the integral of Eq. (23) for the case of a triangular potential with normalized effective mass = 0.1, T = 300 K, field = 10 MV/m, $U_L = U_R$, and $U_{max} - U_L = 0.2$ eV, shown for the transmission coefficients in Fig. 4. (The additional contribution from thermionic emission is not included.)

DISTRIBUTION

1	MS0899	Technical Library	9536 (electronic copy)
1	MS1179	Leonard Lorence	1341 (electronic copy)
1	MS1177	Xujiao Gao	1355 (electronic copy)
1	MS1177	Gary Hennigan	1355 (electronic copy)
1	MS1177	Eric Keiter	1355 (electronic copy)
1	MS1177	Joseph Castro	1355 (electronic copy)
1	MS1315	Normand Modine	1881 (electronic copy)


Sandia National Laboratories